INTERNATIONAL JOURNAL OF HYDROGEN ENERGY XXX (2014) 1–12

Available online at www.sciencedirect.com

ScienceDirect

journal homepage: www.elsevier.com/locate/he

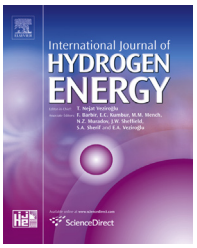

Modeling and optimal design of cyclic processes for hydrogen purification using hydride-forming metals

B.A. Talagañis [a,1,2], G.O. Meyer [b], D.G. Oliva [a,2], M. Fuentes [a,2], P.A. Aguirre [a,*]

[a] Instituto de Desarrollo y Diseño (INGAR), Consejo Nacional de Investigaciones Científicas y Técnicas (CONICET), Avellaneda 3657, S3002GJC Santa Fe, Argentina

[b] Instituto Balseiro, Universidad Nacional de Cuyo, CONICET, Comisión Nacional de Energía Atómica, Centro Atómico Bariloche, Av. Bustillo 9500, S.C. de Bariloche, Argentina

ARTICLE INFO

Article history:
Received 2 July 2014
Received in revised form
5 September 2014
Accepted 8 September 2014
Available online xxx

Keywords:
Modeling
Optimal design
Hydrides
Hydrogen purification

ABSTRACT

Hydrogen at high purity degrees can be obtained by using the well-known Pressure Swing Adsorption (PSA) process. In this paper, a Pressure Swing Absorption (PSAb) alternative operating batch wise is analyzed. An optimal design of cyclic processes for hydrogen purification using hydride-forming metals as absorption material is addressed. The selected case study is a thermo-chemical treatment process that consumes high purity hydrogen to reduce oxides and generates a waste stream that contains residual H_2. PSAb process is fed with this hydrogen-poor stream; and high purity hydrogen recovery levels are obtained. A mathematical model based on an energy integrated scheme is presented to develop the optimal process design and to obtain optimal operating conditions. Various optimized solutions are compared by modifying key parameters or restriction equations. Thus, an interesting trade-off between H_2 recovery and system size is analyzed. Large systems operate at large cycle times, obtaining up to 98% of H_2 recovery in the order of hours, whereas small systems can recover up to 60% of H_2 in short cycles of a few seconds.

Introduction

Unlike the well-known Pressure Swing Adsorption (PSA) process [1] where impurities are retained by adsorption, the process here presented is based on Pressure Swing Absorption (PSAb), where hydrogen undergoes Adsorption, Absorption, and Chemical Reaction with the solid phase. Impurities remain in the gas phase and are expelled against a lower pressure system.

Hydride-forming metals have been used as (solid phase) absorption material for hydrogen storage processes. Versatility of hydride-forming materials has generated a variety of potential applications. These applications range from

* *Corresponding author*. Tel.: +54 342 4555229; fax: +54 342 4553439.
E-mail address: paguir@santafe-conicet.gov.ar (P.A. Aguirre).
[1] Post-mortem publication.
[2] Tel.: +54 342 4555229; fax: +54 342 4553439.
http://dx.doi.org/10.1016/j.ijhydene.2014.09.045

Nomenclature

t	time, s
m	mass, kg
f	gas flow, kg s^{-1}
r	reaction rate, kg_{MH} kg_S^{-1} s^{-1}
T	temperature, K
P	pressure, bar
A	heat interchange area, m^2
V	volume, m^3
U	overall heat transfer coefficient, W m^{-2} K^{-1}
ΔH	enthalpy, J mol^{-1}
ΔS	entropy, J mol^{-1} K^{-1}
C	kinetic constant, s^{-1}
E	activation energy, J mol^{-1}
c_p	specific heat, J kg^{-1} K^{-1}
R	universal gas constant, J mol^{-1} K^{-1}
MW	molecular weight, kg mol^{-1}
SC	stoichiometric coefficient
sl	plateau slope coefficient
imp	impurities percentage
d	diameter
FC	flow coefficient
k	specific heat ratio (const press./const vol.)
φ	flow rate parameter

Subscripts

a	absorption
v	venting
d	desorption
k	stage index
eq	equilibrium
H_2	hydrogen
CO_2	carbon dioxide
MH	metal hydride
S	solid
g	gas
w	refrigerating/heating water
in	inlet
out	outlet
int	internal
ext	external
ini	initial
fin	final

hydrogen storage and compression devices – which are already commercially available – to less developed applications that can make use of low grade heat; for example, heat pumps, refrigeration systems, and hydrogen purification. The relevance of hydride-forming materials has brought about a huge amount of publications regarding different areas of hydrogen technology such as hydrogen storage materials and devices [2–9], hydrogen compression systems [10–18], hydrides characterization devices [19,20], heat pumps [21–23], refrigeration systems [24,25] and purification processes [26–31], among others.

As shown, the available literature includes extensive theoretical and experimental research concerning different aspects of metal hydrides technology and characterization. However, research on hydrogen purification processes is just experimental, and no theoretical studies have been undertaken. Therefore, the objective of this work is to develop a suitable model of the hydrogen purification process and to make use of this model in an optimal process design and operation.

The model concerning hydrogen purification is based on a recently published work in which we developed a simple lumped model. This model consists of a set of differential and algebraic equations, which were used to simulate cyclic processes of pure hydrogen absorption and desorption [32]. This model was fully validated by comparing its outcomes with numerical results and experimental data reported in the literature. The present work provides an extension of the model concerning pure hydrogen to a model considering a gas mixture that contains hydrogen. This was accomplished by adding some specific equations which take into account the presence of a non reactive gas mixed with hydrogen during absorption and desorption chemical reactions. For this purpose, CO_2 is assumed to be the non reactive gas to be used. A mathematical model of a cyclic purification process that involves two reactors working out of phase and coupled with a thermal treatment is also presented.

The paper is organized as follows: a process description that includes operation sequencing is presented in Section Principle of operation and process. The energy integration scheme between asynchronous purification reactors is described in Section Energy integration. Main assumptions and model equations are presented in Section Mathematical model. Results of model implementation and solution are discussed in Section Results and discussion. Finally, conclusions are drawn in Section Conclusions.

Principle of operation and process description

At a definite temperature, a hydrogen storage material has a definite equilibrium pressure which increases exponentially with temperature. Let us suppose there is a reactor filled with hydride-forming material and a hydrogen gas stream is supplied to the reactor. In contrast to conventional PSA in which streams flow through the reactor, no stream leaves the system during absorption in PSAb. When the hydrogen-containing gas comes into contact with the hydride-forming material bed, and if hydrogen partial pressure of gas is higher than the material equilibrium pressure, then the material reacts selectively with hydrogen to form metal hydride. Additional feeding gas enters the reactor during absorption. Gas content that does not react with the material remains in the reactor gas phase. Inert components increase their partial pressure inside the reactor. When the desired hydrided fraction of the bed has been reached, gas supply is closed and then a rapid evacuation of the remaining gases inside the reactor is performed (venting). After that, purified hydrogen can be desorbed from the hydride, reducing the system pressure. By this procedure, hydrogen can be successfully separated from a mixture of gases. The well-known traditional PSA operates each bed in flow mode, whereas the process here presented operates batch wise.

Please cite this article in press as: Talagañis BA, et al., Modeling and optimal design of cyclic processes for hydrogen purification using hydride-forming metals, International Journal of Hydrogen Energy (2014), http://dx.doi.org/10.1016/j.ijhydene.2014.09.045

Fig. 1 shows a hydrogen purification process coupled with an industrial process, which is the source of impure hydrogen. The industrial process consists of a thermal treatment performed at high temperature (900 °C) inside a furnace. The furnace requires a continuous inlet stream of 2 kg/h (0.00056 kg/s) high purity hydrogen in order to produce a reducing atmosphere. Exhaust hydrogen from the furnace contains 2.15 mass% of impurities (CO_2). The objective of the purification process is to capture this impure hydrogen coming from the furnace, separate hydrogen from impurities, expel impurities and re-inject the purified hydrogen into the furnace.

The purification process contains two reactors filled with a well-known hydride-forming material ($LaNi_5$) and several auxiliary devices, namely compressor, heat exchangers, actuated valves, pressure controllers, and pressure regulators. A reservoir filled with fresh pure hydrogen is also needed in order to obtain an amount of hydrogen equivalent to that of hydrogen lost during the purification process (see Fig. 1).

The purification process is cyclic and is coupled with the thermal treatment process. In order to guarantee continuous hydrogen flow into the furnace, the purification process contains two chemical reactors working out of phase. In other words, while one of the reactors is receiving impure hydrogen from the furnace, the other reactor is either desorbing pure hydrogen which is re-injected into the furnace or venting impurities into the atmosphere. During venting, hydrogen needed in the furnace is supplied by the pure hydrogen reservoir.

The purification process consists of three stages performed out of phase in each reactor: absorption, venting, and desorption. A simplified scheme of process configuration and operation sequencing is represented in Fig. 2. These stages are explained below.

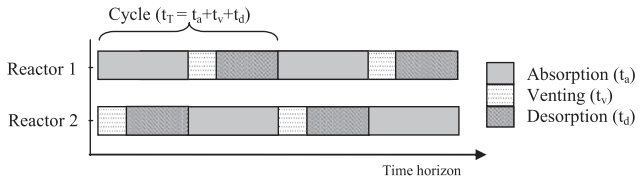

Fig. 2 – : Scheme of operation sequencing.

Absorption stage

Absorption stage in Reactor 1 (R1) begins by opening V1 (see Fig. 1). During this stage, impure hydrogen coming from the furnace is continuously introduced into the reactor by the compressor. An upstream pressure controller guarantees that the gas stream extracted from the furnace is 2 kg/h. Part of the reactor volume is occupied by hydride-forming material (solid) while the remaining part is occupied by gases (hydrogen and impurities). As absorption reaction progresses, gaseous hydrogen is continuously absorbed by the solid material; i.e. it is converted into solid, while impurities remain in gaseous phase. Hence, impurities concentration in gaseous phase is continuously increased while hydrogen concentration is decreased. Absorption stage is interrupted when solid material is partially hydrided. Determination of the optimal duration of each stage as well as the optimal hydrided/dehydrided fraction is one of the goals of the optimization analysis.

As absorption reaction is exothermic and reaction heat is high; reactor must be continuously refrigerated during this stage by a water circulation loop in order to keep equilibrium pressure below hydrogen partial pressure (see Fig. 1).

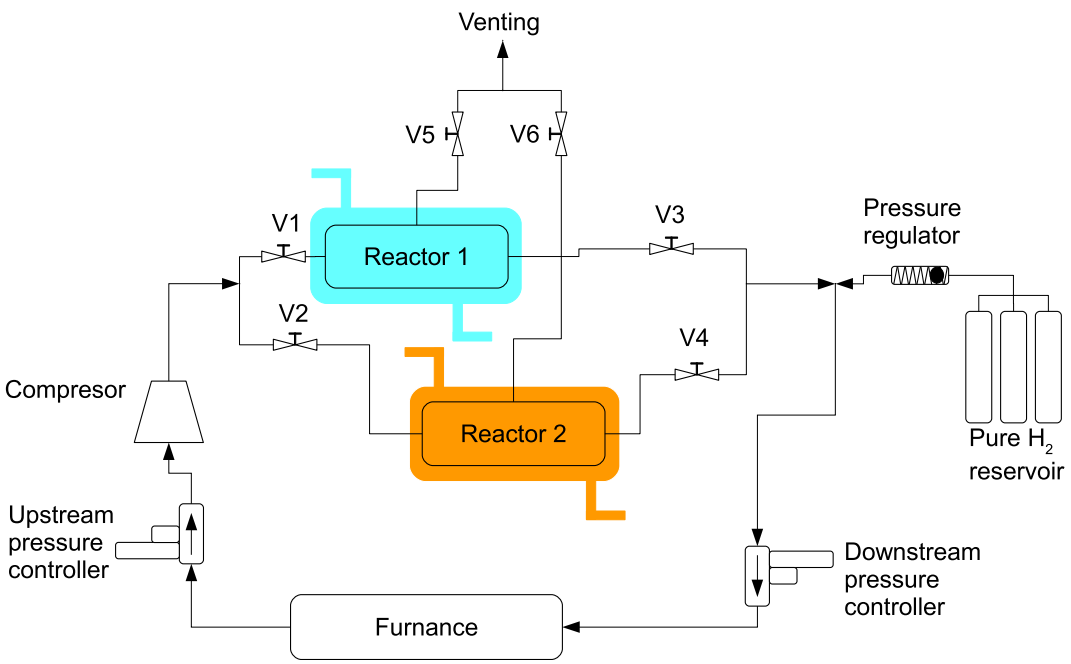

Fig. 1 – : Schematic draw of the purification process with cooling and heating facilities.

Please cite this article in press as: Talagañis BA, et al., Modeling and optimal design of cyclic processes for hydrogen purification using hydride-forming metals, International Journal of Hydrogen Energy (2014), http://dx.doi.org/10.1016/j.ijhydene.2014.09.045

Venting stage

Absorption stage in R1 is finished by closing V1. At the same time, V5 and V2 are opened. By this procedure, venting stage begins in R1 and absorption stage begins in Reactor 2 (R2). The remarkable feature of the venting stage is the continuous exit of gases through a calibrated orifice. When this stage begins, the valve that closes the orifice (V5 for R1) is opened for the gases inside the reactor to flow out into the atmosphere; and pressure inside the reactor rapidly drops. This gas escape causes hydrogen partial pressure inside the reactor to descend below equilibrium pressure value and, therefore, hydride begins to decompose (desorption reaction). Desorption of hydrogen during the venting stage allows reducing the concentration of impurities by diluting them with desorbed pure hydrogen, which leads to extremely high levels of hydrogen purification. The venting stage finishes when the desired level of purity is reached. At that moment, valve V5 corresponding to the calibrated orifice is closed, and V3 is opened.

Desorption stage

When V3 is opened, pressure at the furnace inlet is lower than equilibrium pressure, which improves the desorption stage. A downstream pressure controller guarantees that the gas stream injected into the furnace is 2 kg/h. If desorption rate is lower than 2 kg/h, additional hydrogen is automatically supplied by the pure hydrogen reservoir. R1 desorption stage continues until the optimal dehydrided fraction is reached. Absorption stage takes place simultaneously (V2 being opened and V4/V6 being closed) in R2. R1 desorption stage is finished by closing V3. At the same time, V1 is opened so that absorption stage begins in R1; V2 is closed so that absorption stage finishes in R2; and V6 is opened so that venting stage begins in R2. In this way, a complete cycle is accomplished.

During desorption stage, the corresponding reactor is heated by a water circulation loop in order to keep temperature high enough to allow desorption reaction. The required level of purity for this application is high (1×10^{-4} mass%). Hence, desorption stage is assumed to deal with pure hydrogen.

Energy integration

The schematized process shown in Fig. 1 requires heating and cooling facilities in order to maintain reactors at low temperature during the absorption stage and keep reactors at high temperature during venting and desorption stages. An alternative process configuration is depicted in Fig. 3.

This process executes the purification cycle by performing the same steps explained in previous paragraphs without the requirement of heating and cooling facilities. This is accomplished by coupling both reactors in a single heat exchanger; and energy integration is achieved by making reactors work out of phase. In other words, while the exothermic stage (absorption) is taking place in one of the reactors, endothermic stages (desorption and venting) simultaneously occur in the other one. As a consequence, a minimal supply of energy is required, just enough to recover losses and to balance the small difference between absorption and desorption enthalpies. This energy is supplied by forcing water of the heat exchanger to circulate through an auxiliary heat interchanger (see Fig. 3).

At this point, it should be noted that for large cycle times (i.e. higher amount of solid material), heat exchange with the

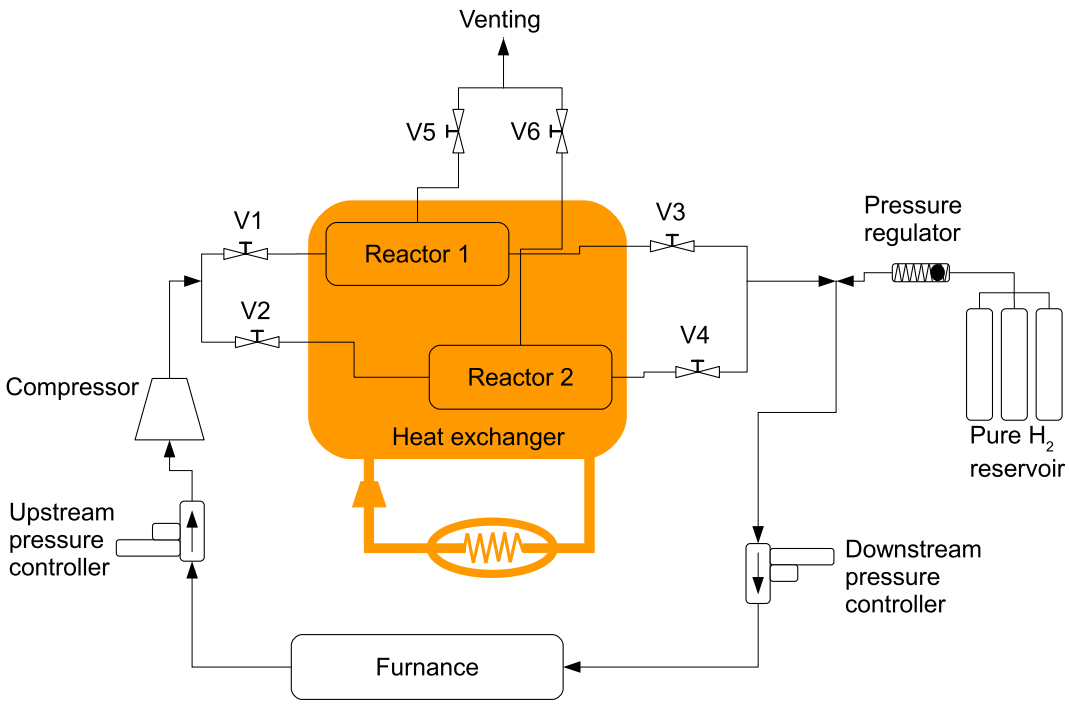

Fig. 3 – : Schematic draw of the purification process with energy integration.

Please cite this article in press as: Talagañis BA, et al., Modeling and optimal design of cyclic processes for hydrogen purification using hydride-forming metals, International Journal of Hydrogen Energy (2014), http://dx.doi.org/10.1016/j.ijhydene.2014.09.045

external fluid is the main thermal phenomenon. For short cycle times, however, thermal capacity of solid material plays a great role in balancing energy among absorption and desorption steps inside the reactor. Solid material reaches high values of temperature at the final point of absorption stage. This high temperature level is optimal for the next steps of venting and desorption. During desorption, solid material undergoes a decrease in temperature. Then, this low temperature value is optimal for the next step of absorption. These compromises will be further clarified by analyzing the solutions obtained with the proposed model.

Mathematical model

The model is based on a recently published work in which we developed a simple lumped model composed of a set of differential and algebraic equations, which was used to simulate a cyclic process of absorption and desorption of pure hydrogen [32]. This model was fully validated by comparing its outcomes with numerical results and experimental data reported in the literature. The model concerning pure hydrogen is extended to the model considering impure hydrogen by adding some specific equations which take into account the presence of a non reactive gas mixed with hydrogen during absorption and desorption chemical reactions. The non reactive gas is assumed to be carbon dioxide (CO_2). A more detailed explanation of the basic equations is found in Ref. [32].

The differential and algebraic equations system is numerically solved by using GAMS (General Algebraic Modeling System) [33]. Generalized reduced gradient algorithm CONOPT3 is selected to solve the nonlinear programming (NLP) problem.

The trapezoidal method was used to discretize ordinary differential equations (ODE). The trapezoidal method is an implicit method for numerically solving initial value problems for ordinary differential equations. It provides an approximate step-by-step solution in discrete increments across the integration interval. Further details can be found in Ref. [32].

Reactors are modeled as cylindrical tubes filled with porous $LaNi_5$. Reactors are cooled during absorption stage and heated during venting/desorption stages by flowing water on their external surfaces. The developed mathematical model is based on the following assumptions:

- Temperature and pressure are average values in radial and axial directions in the reactor. In this way, average temperature and pressure are time-dependent variables.
- Ideal gas law holds in the gas phase.
- Porous medium is homogeneous and isotropic.
- Radiative heat transfer is negligible.
- Volume of gas phase, solid phase, and reactor are constant.
- Physical properties of the hydride bed are independent of temperature and hydrogen pressure.
- Constant atmospheric pressure and constant gas flow rate are established at the output orifice during venting.
- No diffusional limitations in the gas phase are assumed. For particles of 1×10^{-4} m diameter and 0.1 m diffusional length, Damköhler number is in the order of 1×10^{-3}.

The use of average temperatures and pressures allows simplifying the model. Reactors with an inert phase of high thermal conductivity allow reducing thermal variation along the reactor. Cooper chips or leads, or metal sponges help to increase global thermal conductivity. Alternatively, small reactor diameters lead to high heat exchange rates and reduced temperature gradients. As a result, the equations describing mass and energy balances are ordinary differential equations rather than partial differential equations. Average temperature and composition, then, are used in mass and energy balances. Calculations of bed and gas properties are averaged too. Calculations for average heat transfer coefficients involve the computation of global heat transfer coefficient by using reactor average temperature.

Considering these assumptions, the equations governing heat and mass transfer in the metal–hydrogen reactor are the following:

Mass balance equations are written for gaseous hydrogen, impurities (CO_2), and metal hydride. Subscript k refers to absorption, venting, or desorption stages.

$$\frac{dm_{H_2\_k}}{dt} = \varphi_{in\_H_2\_k} f_{in\_H_2\_k} - \varphi_{out\_H_2\_k} f_{out\_H_2\_k} - r_k m_S \frac{MW_{H_2} SC}{MW_{MH}} \quad (1)$$

$$\frac{dm_{CO_2\_k}}{dt} = \varphi_{in\_CO_2\_k} f_{in\_CO_2\_k} - \varphi_{out\_CO_2\_k} f_{out\_CO_2\_k} \quad (2)$$

$$\frac{dm_{MH\_k}}{dt} = r_k m_S \quad (3)$$

Equilibrium pressure is modeled using van't Hoff equation. According to this equation, plateau pressure of an ideal hydride only depends on material properties and temperature. Nonetheless, a constant slope term is usually added to approximate to real material behavior [34]. Equilibrium pressure is then a function of temperature and hydrogen concentration and can be represented as follows:

$$P_{eq\ k} = e^{\left(\frac{\Delta H_k}{RT_k} - \frac{\Delta S_k}{R} + sl_k\left(\frac{m_{MH\_k}}{m_S} - 0.5\right)\right)} P_0 \quad (4)$$

Parameters ΔH_k, ΔS_k, and sl_k, are the same for venting and desorption stages. Extensive studies have led to different conclusions on the type of kinetics and controlling mechanisms being involved during absorption and desorption reactions. However, there exists a widely accepted model which is successfully used for the case of $LaNi_5$–H_2 system. Reaction rate expressions for each k-stage are summarized in Table 1.

One usual assumption in most studies is considering gas phase temperature equal to solid phase temperature. Then, a single energy balance equation is sufficient to determine temperature in the reactor:

$$\begin{aligned}(m_{H_2\_k} c_{pH_2} + m_{CO_2\_k} c_{pCO_2} + m_S c_{pS}) \frac{dT_k}{dt} \\ = \left(\varphi_{in\_H_2\_k} f_{in\_H_2 k} c_{pH_2} + \varphi_{in\_CO_2\_k} f_{in\_CO_2 k} c_{pCO_2}\right)(T_{in} - T_k) \\ + AU(T_{w\_k} - T_k) + \Delta H_k r_k m_S \frac{SC}{MW_{MH}}\end{aligned} \quad (5)$$

State equations for gaseous hydrogen and for CO_2 are needed in order to relate gas partial pressures with the corresponding masses of the substances in the system:

Please cite this article in press as: Talagañis BA, et al., Modeling and optimal design of cyclic processes for hydrogen purification using hydride-forming metals, International Journal of Hydrogen Energy (2014), http://dx.doi.org/10.1016/j.ijhydene.2014.09.045

Table 1 – Reaction rate expressions and flow rate parameter matrix.

Stage (k)	Reaction rate (r_a)	$\varphi_{in\_H_2\_k}$	$\varphi_{out\_H_2\_k}$	$\varphi_{in\_CO_2\_k}$	$\varphi_{out\_CO_2\_k}$
Absorption ($k=a$)	$r_a = C_a e^{-E_a/RT_a} \ln\left(\frac{P_{H_2\,a}}{P_{eq\,a}}\right)\left(1-\frac{m_{MH\,a}}{m_S}\right)$	1	0	1	0
Venting ($k=v$)	$r_v = C_d e^{-E_d/RT_v}\left(\frac{P_{H_2\,v}-P_{eq\,v}}{P_{eq\,v}}\right)\left(\frac{m_{MH\,v}}{m_S}\right)$	0	1	0	1
Desorption ($k=d$)	$r_d = C_d e^{-E_d/RT_d}\left(\frac{P_{H_2\,d}-P_{eq\,d}}{P_{eq\,d}}\right)\left(\frac{m_{MH\,d}}{m_S}\right)$	0	1	0	0

$$m_{H_2\_k} = \frac{P_{H_2\_k} V_g MW_{H_2}}{RT_k} \tag{6}$$

$$m_{CO_2\_k} = \frac{P_{CO_2\_k} V_g MW_{CO_2}}{RT_k} \tag{7}$$

Total pressure inside reactor results from the addition of gaseous component partial pressures:

$$P_{H_2\_k} + P_{CO_2\_k} = P_k \tag{8}$$

Relationships among mass and mass flow of H_2 and CO_2 and impurities concentration (imp_k) are written as:

$$imp_k = \frac{m_{CO_2\_k}}{m_{CO_2\_k} + m_{H_2\_k}} 100 \tag{9}$$

$$f_{in\ or\ out\_H_2\_k} = \left(\frac{100}{imp_k} - 1\right) f_{in\ or\ out\_CO_2\_k} \tag{10}$$

The process is designed to absorb hydrogen coming from the furnace. The following equation establishes this requirement:

$$consumption\_H_{2_a} = r_a m_S \frac{MW_{H_2} SC}{MW_{MH}} \tag{11}$$

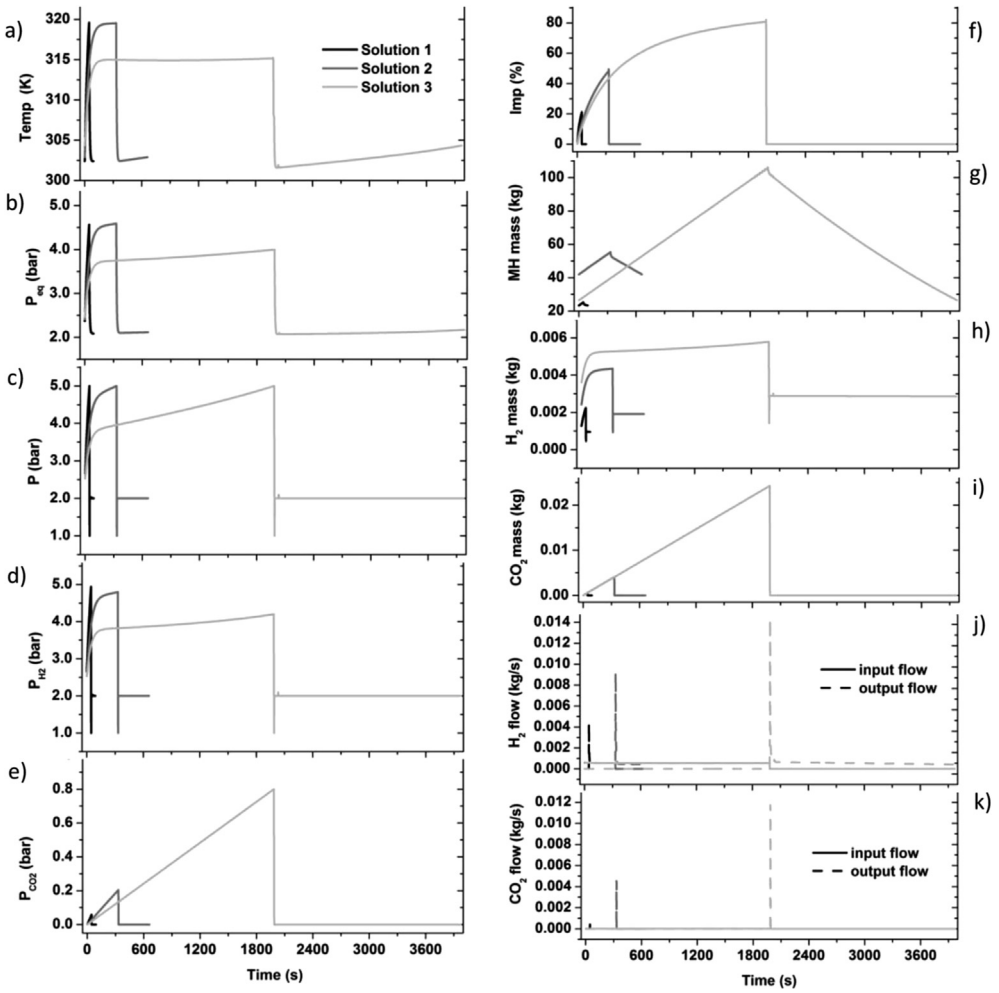

Fig. 4 – : Predicted values for three optimized solutions (m_s equal 50, 100 and 150 kg).

Please cite this article in press as: Talagañis BA, et al., Modeling and optimal design of cyclic processes for hydrogen purification using hydride-forming metals, International Journal of Hydrogen Energy (2014), http://dx.doi.org/10.1016/j.ijhydene.2014.09.045

Initial conditions and linking/auxiliary equations are summarized in Appendix A.

Results and discussion

As already mentioned, the equations system described in the previous section is solved by using optimization software "GAMS" (General Algebraic Modeling System). The optimization objective function is maximizing H_2 recovery percentage. This recovery percentage is limited by the hydride-forming material mass (or "solid mass", "m_s") located in reactors. Higher H_2 recovery percentages can be reached by locating a higher amount of m_s. However, a higher amount of m_s means a more expensive system, not only because of hydride cost but also because more hydride mass means a bigger and more expensive structure. Optimization solutions for different m_s help to solve this trade-off. If hydrogen price and structure cost for different sizes are known, then the optimization analysis provides the optimal size of the system to be installed and also the appropriate operation parameters, i.e. duration of cycle stages, temperature of heating/cooling fluid, pressures, etc.

Fig. 4 shows time evolution during a complete purification cycle of several key variables for three different optimized solutions.

- Solution 1 (solid line in Fig. 4): for this solution, m_S is restricted to 50 kg. For this restriction, cycle time is about 1.5 min; and a 77.48% H_2 recovery can be achieved. In this solution, heat exchange with circulating fluid plays a secondary role.
- Solution 2 (dashed line): m_S is restricted to 100 kg, resulting in a 92.52% H_2 recovery and an 11-min cycle time.
- Solution 3 (dotted line): m_S is restricted to 150 kg, resulting in a 97.85% H_2 recovery. Cycle time for this condition is 66 min. In solutions 2 and 3, heat exchange with circulation fluid plays a central role in temperature control and, hence, in process performance.

Fig. 4a shows the evolution of average bed temperature throughout the cycle. Bed temperature at the beginning of absorption stage is low. When gaseous hydrogen flows into the reactor, exothermic hydriding reaction begins and so solid bed temperature increases. Increased bed temperature causes a corresponding increase of material equilibrium pressure and total pressure inside reactor (Fig. 4b and c, respectively). Equilibrium pressure is always below H_2 partial pressure during absorption stage (Fig. 4d); otherwise, absorption reaction would stop. When absorption stage finishes, venting stage begins. At this moment, the rapid gases evacuation causes an abrupt pressure drop inside reactor (Fig. 4c). Consequently, system pressure falls below equilibrium pressure and desorption reaction begins. During venting stage, desorption rate is high and heat is consumed by reaction. Hence, bed temperature diminishes abruptly (Fig. 4a). It should be noted that there is a structural difference between case 1 and the other cases for temperature pattern. Reactor temperature in cases 2 and 3 shows large plateau with constant value, whereas temperature in case 1 did not.

Fig. 4e shows the evolution of CO_2 partial pressure during the cycle. As it can be seen, during absorption stage, CO_2 partial pressure increases linearly because CO_2 mixed with H_2 is continuously being introduced into the reactor. During venting stage, CO_2 is expelled into the atmosphere, achieving the objective of the system (hydrogen purification). As a result, CO_2 partial pressure is almost zero during desorption stage. This effect is also shown in Fig. 4f, considering mass % of impurities (CO_2) in the gas phase.

Fig. 4g shows metal hydride mass evolution. This illustrates that hydride-forming material m_S is only partially hydrided/dehydrided. Optimization analysis shows the importance of the existing trade-off in a complete absorption/desorption cycle in relation to the convenience of stopping both absorption and desorption stages long before the hydride-forming material is fully hydrided or dehydrided. As it can be seen, for Solution 1 only a small fraction of hydride-forming material reacts reversibly with H_2 to form hydride. On the other hand, this fraction is elevated for Solution 3. The values for the three cases are the following:

- Solution 1: hydride material mass in reactor is 50 kg; the optimal solution of the model for this case gives an initial hydrided mass of 23.39 kg (this is hydrided mass before absorption). After absorption, final hydrided mass is 25.22 kg. In the optimal solution, then, only 3.66% of the material reacts during the cycle.
- Solution 2: hydride material mass in reactor is 100 kg; the optimal solution of the model for this case gives an initial hydrided mass of 42.04 kg (this is hydrided mass before absorption). After absorption, final hydrided mass is

Table 2 – Parameters used in computations.

Parameter	Value	Units
Material	$LaNi_5$	
ΔH_a	−30478	J $mol_{H_2}^{-1}$
ΔH_d	30,800	J $mol_{H_2}^{-1}$
ΔS_a	−108	J $mol_{H_2}^{-1}$ K^{-1}
ΔS_d	108	J $mol_{H_2}^{-1}$ K^{-1}
E_a	21,170	J $mol_{H_2}^{-1}$
E_d	16,420	J $mol_{H_2}^{-1}$
C_a	59.2	s^{-1}
C_d	9.6	s^{-1}
sl_a	0.13	
sl_d	0.13	
MW_{MH}	0.432	kg_{MH} mol_{MH}^{-1}
MW_{H_2}	0.002	kg_{H_2} $mol_{H_2}^{-1}$
MW_{CO_2}	0.044	kg_{H_2} $mol_{H_2}^{-1}$
c_{pS}	355	J kg_S^{-1} K^{-1}
c_{pH_2}	14,300	J $kg_{H_2}^{-1}$ K^{-1}
U_a	243	W m^{-2} K^{-1}
U_v	243	W m^{-2} K^{-1}
U_d	243	W m^{-2} K^{-1}
consumption_H_{2_a}	0.00056	$kg_{H_2}^{-1}$ s^{-1}
imp_{in}	2.15	mass%
$Imp_{admissible}$	0.0022	mass%
FC	0.62	
k	1.38	
R	8.314	J $mol_{H_2}^{-1}$ K^{-1}
SC	3	mol_{H_2} mol_{MH}^{-1}
P_0	1	bar

Please cite this article in press as: Talagañis BA, et al., Modeling and optimal design of cyclic processes for hydrogen purification using hydride-forming metals, International Journal of Hydrogen Energy (2014), http://dx.doi.org/10.1016/j.ijhydene.2014.09.045

Table 3 – Optimized variable values for Solutions 1, 2 and 3.

	Variable	Solution 1	Solution 2	Solution 3	Units
Reactor design	m_S	50	100	150	kg_S
	V_g	0.006	0.012	0.018	m^3
	A	1.9	3.8	5.7	m^2
Operating conditions	T_{wa}	308.5	310.2	309.0	K
	T_{wv}	308.5	310.2	309.0	K
	T_{wd}	308.5	310.2	309.0	K
	T_{in}	323.4	328.7	326.0	K
	t_a	45.84	330.94	1985.60	s
	t_v	1.85	2.31	3.64	s
	t_d	43.99	328.63	1981.96	s
H_2recovery		77.48	92.52	97.85	%

55.27 kg. In the optimal solution, then, only 33.23% of the material reacts during the cycle.

- Solution 3: hydride material mass in reactor is 150 kg; the optimal solution of the model for this case gives an initial hydrided mass of 26.47 kg (this is hydrided mass before absorption). After absorption, final hydrided mass is 105.89 kg. In the optimal solution, then, 52.96% of the material reacts during the cycle.

Fig. 4h and i, and Fig. 4j and k shows the evolution of gaseous H_2 and CO_2 masses and mass flow, respectively, during the cycle. Model parameters are summarized in Table 2. The optimized variable values resulting from optimization analysis are detailed in Table 3. Average values for water temperature (T_w) are reported.

The presented optimization analysis can be repeated for a wide range of m_S, obtaining the curve shown in Fig. 5. Three points of the curve are highlighted. These points correspond to the solutions that are fully depicted in Fig. 4 and Table 3. This curve shows H_2 recovery percentage as a function of hydride-forming material mass. As shown, higher m_S mass implies higher H_2 recovery. However, as mentioned, a high m_S mass increases purification process costs. Therefore, given the hydrogen price and structure costs, this curve provides the optimal size of the structure to be constructed. Once the optimal structure size has been identified, the optimization analysis also provides the optimal process synthesis and operation parameters similar to those shown in Table 3.

Similar curves can be obtained by modifying key parameters or restriction equations. Solutions corresponding to these modifications provide more information about the behavior of the process when conditions are varied. Figs. 6 and 7 show curves corresponding to the following modifications performed over the original situation exposed in Fig. 5:

- Case 1: original case is included in Figs. 6 and 7 for comparison.
- Case 2: the scheduling equation (Eq. (A.17)) is removed. Thus, the solution for this case is called "relaxed". This relaxation allows achieving higher H_2 recovery percentages for the same m_S value. However, removing this restriction causes that the process is no longer scheduled, so that auxiliary storage tanks might be necessary in order to assure continuous production.
- Case 3: parameter "$imp_{admissible}$" is increased one order of magnitude, i.e. from 0.0022 to 0.022 mass%. This condition allows higher H_2 recovery, but to the detriment of recovered hydrogen purity level.
- Case 4: parameter "imp_{in}", i.e. impurity level in the absorption inlet gaseous stream, undergoes a 400% increase (from 2.15 to 8.6 mass%). This condition causes lower H_2 recovery. However, this case shows that the process can

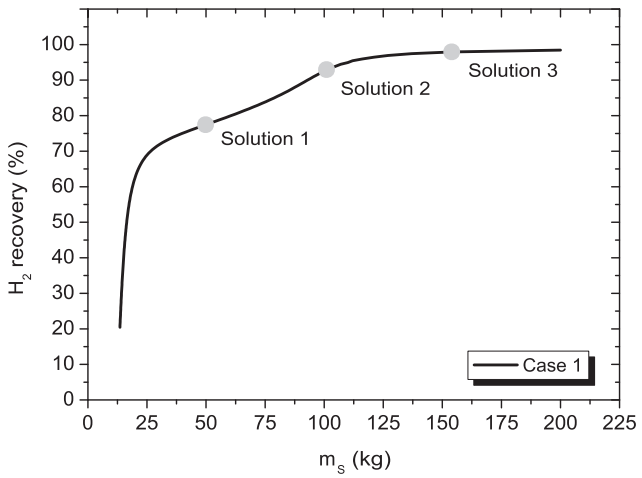

Fig. 5 – : Optimal solutions for different m_S values (Case 1).

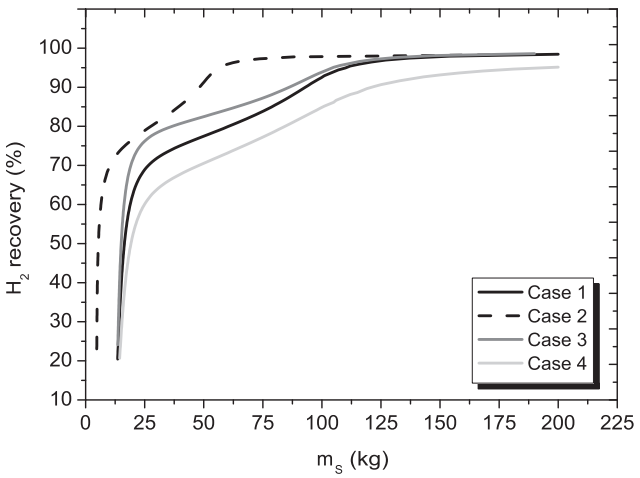

Fig. 6 – : Comparison of optimization Cases 1, 2, 3 and 4.

Please cite this article in press as: Talagañis BA, et al., Modeling and optimal design of cyclic processes for hydrogen purification using hydride-forming metals, International Journal of Hydrogen Energy (2014), http://dx.doi.org/10.1016/j.ijhydene.2014.09.045

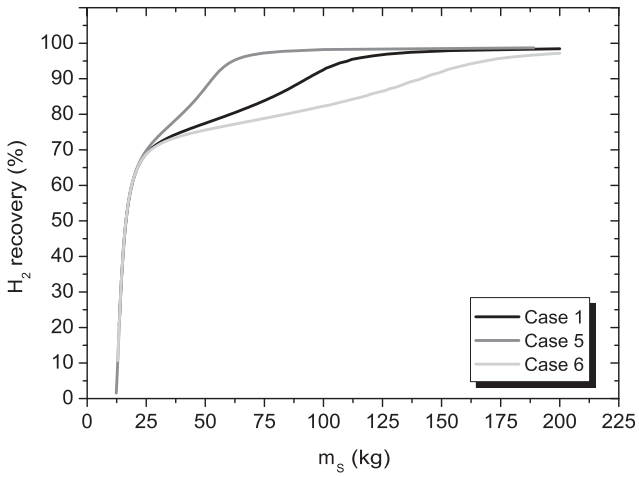

Fig. 7 – : Comparison of optimization Cases 1, 5 and 6.

work quite satisfactory even if impurity inlet value is significantly increased.

- Cases 5 and 6: global heat transfer coefficient "U" ($U = U_a = U_v = U_d$) is increased from 243 to 500 W m^{-2} K^{-1} in Case 5; and it is decreased from 243 to 150 W m^{-2} K^{-1} in Case 6. Fig. 7 shows the comparison between cases 1, 5, and 6. This figure depicts that higher heat transfer coefficient improves the process behavior, i.e. H_2 recovery is higher. For low m_S values, the process behavior is relatively independent of U value. In addition, for low m_S values, the system seems to present a minimum required m_S even for very low H_2 recovery percentages. For these values, process time and hydrided/dehydrided fraction are very small and, consequently, heat caused by reaction is also very low.

Energy behavior in the absorption process is presented in Fig. 8. It should be noted that, for low m_S values (i.e. short cycle times), the energy generated by reaction $\left(\Delta H_a r_a m_S \frac{SC}{MW_{MH}} dt\right)$ is mainly absorbed by the hydride-forming material ($m_S c_{pS} dT_v$). Contrarily, for high m_S values (i.e. long cycle times), the energy generated by reaction is mainly transferred to the heating/cooling water ($AU(T_{w\,a} - T_a)dt$).

Conclusions

A computational study of hydrogen purification processes that use hydride-forming metals was presented in this work. A suitable cyclic process for hydrogen purification was designed and modeled. The cyclic purification process was performed by two chemical reactors that were scheduled and worked out of phase; and it is based on Pressure Swing Absorption process and interconnected with a continuous thermal treatment process.

The model considers impure hydrogen, i.e. takes into account the presence of a non reactive gas (CO_2) mixed with hydrogen during absorption and desorption chemical reactions. This model consists of a set of differential and algebraic equations which were solved using GAMS optimization software.

Three solutions were analyzed when hydrogen recovery was optimized for 25, 50, and 75 $kg_{metal\ hydride}/(kg_{hydrogen}/h)$ (i.e. kg of metal hydride material by kg of hydrogen fed to the reactor per hour). Hydrogen recovery, cycle duration, and hydride mass usage percentage in the solutions were: 66, 88, and 98%; 1.5, 11, and 66 min; and 3.6, 13.23, and 52.96%, respectively. Temperatures in the input gas stream, purification reactors, and cooling/heating water ranged from 323.4 to 328.7, 300 to 320, and 308.5 to 310.2 K, respectively.

Hydride mass versus hydrogen recovery profiles were presented for six cases by varying some parameters. A first case was used for representing the standard operation of the case study. A heat transfer analysis during the absorption process in this case revealed that for operative values lower than 25 $kg_{metal\ hydride}/(kg_{hydrogen}/h)$ the energy generated by the reaction process was mainly used by the hydride material to increase its temperature. From 25 to 45 $kg_{metal\ hydride}/(kg_{hydrogen}/h)$, energy is shared for temperature increases of hydride material and (heating/cooling) water. For operative conditions greater than 45 $kg_{metal\ hydride}/(kg_{hydrogen}/h)$, energy is mainly transferred to the heating/cooling water. The second case, without scheduling restrictions, showed the best hydrogen recovery for a given metal hydride mass; but auxiliary storage tanks are necessary in order to assure continuous production. In the third case, admissible impurities in recovered hydrogen are increased one order of

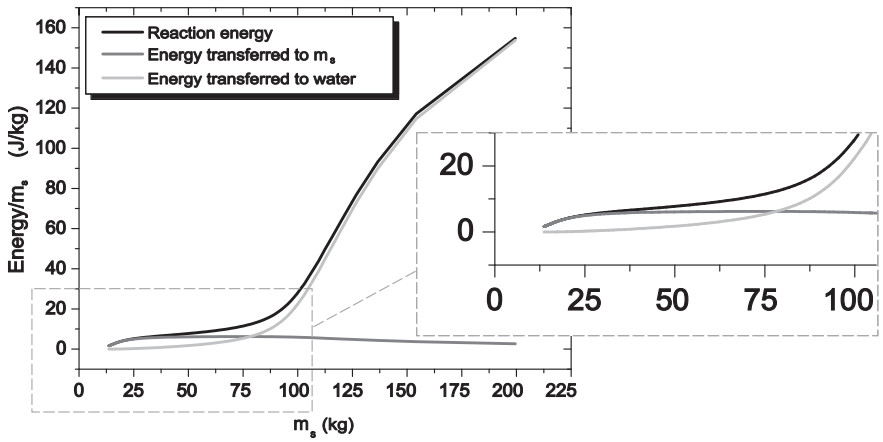

Fig. 8 – Energies involved in the absorption process.

Please cite this article in press as: Talagañis BA, et al., Modeling and optimal design of cyclic processes for hydrogen purification using hydride-forming metals, International Journal of Hydrogen Energy (2014), http://dx.doi.org/10.1016/j.ijhydene.2014.09.045

magnitude, resulting in an increase in the hydrogen recovery for operative values from 10 to 75 $kg_{metal\ hydride}/(kg_{hydrogen}/h)$. In the fourth case, input impurity specification was varied. When input impurities increase, a linear decrease in hydrogen recovery and an exponential decrease of the cycle time are observed in/under operating conditions greater than 10 $kg_{metal\ hydride}/(kg_{hydrogen}/h)$. The fifth and sixth cases were proposed to evaluate process behavior when global heat transfer coefficient is modified. It is observed that hydrogen recovery variations were significant for operative values greater than 10 $kg_{metal\ hydride}/(kg_{hydrogen}/h)$.

Future works are oriented to study and compare this process with other currently available processes (e.g. PSA). It would be very interesting to undertake further research on model integration in energy production systems based on hydrogen consumption (e.g. proton exchange membrane fuel cell system).

Acknowledgments

The authors acknowledge financial support provided by Consejo Nacional de Investigaciones Científicas y Técnicas (CONICET), Universidad Nacional del Litoral, Universidad Tecnológica Nacional, and Agencia Nacional de Promoción Científica y Tecnológica (ANPCyT) of Argentina.

Appendix A. Initial conditions and linking/auxiliary equations.

Since hydride-forming material mass (m_s) is an optimization variable, two equations should be included to consider the increment or decrease of reactor volume and heat transfer area when m_S is varied [32]:

$$V_g = m_S/8300 \tag{A.1}$$

$$A = 4V_g/0.0127 \tag{A.2}$$

The venting orifice diameter (d_v) defines gases velocity in the orifice. This velocity should be high enough to ensure that no gas from the exterior enters the reactor during venting. This requirement is modeled with the following equations [35]:

$$f_{out\_H_2\_v} + f_{out\_CO_2\_v} = -FC3.14\left(\frac{d_v}{2}\right)^2 P_v \sqrt{\frac{2\left(MW_{H_2}\frac{P_{H_2\_v}}{P_v} + MW_{CO_2}\frac{P_{CO_2\_v}}{P_v}\right)}{RT_v}\ \frac{k}{k-1}\left[\left(\frac{P_{ext}}{P_v}\right)^{2/k} - \left(\frac{P_{ext}}{P_v}\right)^{(k+1)/k}\right]} \tag{A.3}$$

$$\text{gas velocity}_v = -\frac{\left(f_{out\_H_2\_v} + f_{out\_CO_2\_v}\right)RT_v}{\left(MW_{H_2}\frac{P_{H_2\_v}}{P_v} + MW_{CO_2}\frac{P_{CO_2\_v}}{P_v}\right)P_{ext}3.14\left(\frac{d_v}{2}\right)^2} \tag{A.4}$$

Hydrogen recovery percentage is obtained from the relation between hydrogen lost during venting stage and hydrogen absorbed during absorption stage:

$$H_2\ \text{recovery} = 100 - 100\left(\frac{m_{MH\_v\ (ini)} - m_{MH\_v\ (fin)}}{m_{MH\_a\ (fin)} - m_{MH\_a\ (ini)}}\right) \tag{A.5}$$

The following equations are used to link stages, i.e. to ensure that the final conditions of a stage are equal to the initial conditions of the next stage in each reactor:

$$T_{a\ (ini)} = T_{d\ (fin)} \tag{A.6}$$

$$T_{v\ (ini)} = T_{a\ (fin)} \tag{A.7}$$

$$T_{d\ (ini)} = T_{v\ (fin)} \tag{A.8}$$

$$m_{MH\_a\ (ini)} = m_{MH\_d\ (fin)} \tag{A.9}$$

$$m_{MH\_v\ (ini)} = m_{MH\_a\ (fin)} \tag{A.10}$$

$$m_{MH\_d\ (ini)} = m_{MH\_v\ (fin)} \tag{A.11}$$

$$m_{CO_2\_a\ (ini)} = 0 \tag{A.12}$$

$$m_{CO_2\_v\ (ini)} = m_{CO_2\_a\ (fin)} \tag{A.13}$$

$$m_{H_2\_v\ (ini)} = m_{H_2\_a\ (fin)} \tag{A.14}$$

$$P_{v(ini)} = P_{a(fin)} \tag{A.15}$$

The following equation forces the venting stage to continue until the desired level of hydrogen purity is reached:

$$imp_{v(fin)} \le imp_{admissible} \tag{A.16}$$

One scheduling equation is included to link stages between reactors R1 and R2, i.e. duration of R1 absorption stage is equal to duration of R2 venting stage plus R2 desorption stage, and vice versa:

$$t_{a_{Ri}} = t_{v_{Rj}} + t_{d_{Rj}} \quad \forall i \neq j,\ i = \{1,2\} \wedge j = \{1,2\} \tag{A.17}$$

For the energy integration case (see Fig. 3), the following equations describe the relationship of heating/cooling water temperatures during stages occurring in reactors R1 and R2 (see Fig. 2):

$$T_{w\_a_{Ri}}\left(t_{v_{Rj}}\right) = T_{w\_v_{Rj}}\left(t_{v_{Rj}}\right) \quad \forall i \neq j,\ i = \{1,2\} \wedge j = \{1,2\} \tag{A.18}$$

$$T_{w\_a_{Ri}}\left(t_{d_{Rj}}\right) = T_{w\_d_{Rj}}\left(t_{d_{Rj}}\right) \quad \forall i \neq j,\ i = \{1,2\} \wedge j = \{1,2\} \tag{A.19}$$

Please cite this article in press as: Talagañis BA, et al., Modeling and optimal design of cyclic processes for hydrogen purification using hydride-forming metals, International Journal of Hydrogen Energy (2014), http://dx.doi.org/10.1016/j.ijhydene.2014.09.045

Equations (A.20) and (A.21) are used to calculate water temperature during *Ri* absorption–*Rj* venting ($t_{v_{Rj}}$) and *Ri* absorption–*Rj* desorption ($t_{d_{Rj}}$) periods, respectively.

$$\left.\frac{dT_{w\_a_{Ri}}}{dt}\right|_{t=t_{v_{Rj}}} = \frac{AU(T_{a_{Ri}} - T_{w\_a_{Ri}}) + AU\left(T_{v_{Rj}} - T_{w\_a_{Ri}}\right)}{m_w C_{pW}} \quad \forall i \neq j,$$
$$i = \{1,2\} \wedge j = \{1,2\} \tag{A.20}$$

$$\left.\frac{dT_{w\_a_{Ri}}}{dt}\right|_{t=t_{d_{Rj}}} = \frac{AU(T_{a_{Ri}} - T_{w\_a_{Ri}}) + AU\left(T_{d_{Rj}} - T_{w\_a_{Ri}}\right)}{m_w C_{pW}} \quad \forall i \neq j,$$
$$i = \{1,2\} \wedge j = \{1,2\} \tag{A.21}$$

Equations (A.18)–(A.21) are difficult to satisfy when solving simulations and optimizations. Careful numerical initializations were performed in order to obtain robust calculation sequences.

REFERENCES

[1] Ruthven DM, Farooq S, Knaebel KS. Pressure swing adsorption. 1st ed. New York, N.Y: Wiley-VCH; 1993.
[2] Ahluwalia RK, Hua TQ, Peng JK. On-board and off-board performance of hydrogen storage options for light-duty vehicles. Int J Hydrogen Energy 2012;37:2891–910. http://dx.doi.org/10.1016/j.ijhydene.2011.05.040.
[3] Souahlia A, Dhaou H, Askri F, Sofiene M, Jemni A, Ben Nasrallah S. Experimental and comparative study of metal hydride hydrogen tanks. Int J Hydrogen Energy 2011;36:12918–22. http://dx.doi.org/10.1016/j.ijhydene.2011.07.022.
[4] Johnson TA, Kanouff MP, Dedrick DE, Evans GH, Jorgensen SW. Model-based design of an automotive-scale, metal hydride hydrogen storage system. Int J Hydrogen Energy 2012;37:2835–49. http://dx.doi.org/10.1016/j.ijhydene.2011.05.030.
[5] Muthukumar P, Linder M, Mertz R, Laurien E. Measurement of thermodynamic properties of some hydrogen absorbing alloys. Int J Hydrogen Energy 2009;34:1873–9. http://dx.doi.org/10.1016/j.ijhydene.2008.12.052.
[6] Talagañis BA, Esquivel MR, Meyer G. Study of annealing effects on structural and sorption properties of low energy mechanically alloyed AB5's. J Alloys Compd 2010;495:541–4. http://dx.doi.org/10.1016/j.jallcom.2009.10.248.
[7] Urretavizcaya G, García G, Serafini D, Meyer G. Mg–Ni alloys for hydrogen storage obtained by ball milling. Lat Am Appl Res 2002;32:289–94.
[8] Krokos CA, Nikolic D, Kikkinides ES, Georgiadis MC, Stubos AK. Modeling and optimization of multi-tubular metal hydride beds for efficient hydrogen storage. Int J Hydrogen Energy 2009;34:9128–40. http://dx.doi.org/10.1016/j.ijhydene.2009.09.021.
[9] Valverde L, Rosa F, del Real AJ, Arce A, Bordons C. Modeling, simulation and experimental set-up of a renewable hydrogen-based domestic microgrid. Int J Hydrogen Energy 2013;38:11672–84. http://dx.doi.org/10.1016/j.ijhydene.2013.06.113.
[10] Wang X, Liu H, Li HA. 70 MPa hydrogen-compression system using metal hydrides. Int J Hydrogen Energy 2011;36:9079–85. http://dx.doi.org/10.1016/j.ijhydene.2011.04.193.
[11] Hopkins RR, Kim KJ. Hydrogen compression characteristics of a dual stage thermal compressor system utilizing $LaNi_5$ and $Ca_{0.6}Mm_{0.4}Ni_5$ as the working metal hydrides. Int J Hydrogen Energy 2010;35:5693–702. http://dx.doi.org/10.1016/j.ijhydene.2010.03.065.
[12] Talagañis BA, Esquivel MR, Meyer G. A two-stage hydrogen compressor based on (La, Ce, Nd, Pr)Ni_5 intermetallics obtained by low energy mechanical alloying – low temperature annealing treatment. Int J Hydrogen Energy 2009;34:2062–8. http://dx.doi.org/10.1016/j.ijhydene.2008.11.052.
[13] Talagañis BA, Esquivel MR, Meyer G. Improvement of as-milled properties of mechanically alloyed $LaNi_5$ and application to hydrogen thermal compression. Int J Hydrogen Energy 2011;36:11961–8. http://dx.doi.org/10.1016/j.ijhydene.2011.06.047.
[14] Koultoukis ED, Gkanas EI, Makridis SS, Christodoulou CN, Fruchart D, Stubos AK. High-temperature activated AB2 nanopowders for metal hydride hydrogen compression. Int J Energy Res 2014;38:477–86. http://dx.doi.org/10.1002/er.3147.
[15] Gkanas EI, Makridis SS, Stubos AK. Modeling and simulation for absorption–desorption cyclic process on a three-stage metal hydride hydrogen compressor. In: Kraslawski Andrzej, Turunen Ilkka, editors. Comput. Aided Chem. Eng, vol. 32. Elsevier; 2013. p. 379–84.
[16] Odysseos M, De Rango P, Christodoulou CN, Hlil EK, Steriotis T, Karagiorgis G, et al. The effect of compositional changes on the structural and hydrogen storage properties of (La–Ce)Ni_5 type intermetallics towards compounds suitable for metal hydride hydrogen compression. J Alloys Compd 2013;580(Suppl. 1):S268–70. http://dx.doi.org/10.1016/j.jallcom.2013.01.057.
[17] Koultoukis ED, Makridis SS, Fruchart D, Stubos AK. Two-stage hydrogen compression using Zr-based metal hydrides. Solid State Phenom 2012;194:249–53. http://dx.doi.org/10.4028/www.scientific.net/SSP.194.249.
[18] Lototskyy MV, Yartys VA, Pollet BG, Bowman Jr RC. Metal hydride hydrogen compressors: a review. Int J Hydrogen Energy 2014;39:5818–51. http://dx.doi.org/10.1016/j.ijhydene.2014.01.158.
[19] Meyer G, Larochette PA, Baruj A, Castro FJ, Lacharmoise P, Zacur E, et al. Equipment for hydrogen absorption–desorption cycling characterization of hydride forming materials. Rev Sci Instrum 2007;78:023903. http://dx.doi.org/10.1063/1.2437160.
[20] Talagañis BA, Castro FJ, Baruj A, Meyer G. Novel device for simultaneous volumetric and X-ray diffraction measurements on metal–hydrogen systems. Rev Sci Instrum 2009;80:073901. http://dx.doi.org/10.1063/1.3157086.
[21] Satheesh A, Muthukumar P. Performance investigation of double-stage metal hydride based heat pump. Appl Therm Eng 2010;30:2698–707. http://dx.doi.org/10.1016/j.applthermaleng.2010.07.021.
[22] Satheesh A, Muthukumar P. Performance investigations of a single-stage metal hydride heat pump. Int J Hydrogen Energy 2010;35:6950–8. http://dx.doi.org/10.1016/j.ijhydene.2010.04.043.
[23] Satheesh A, Muthukumar P. Simulation of double-stage double-effect metal hydride heat pump. Int J Hydrogen Energy 2010;35:1474–84. http://dx.doi.org/10.1016/j.ijhydene.2009.12.027.
[24] Satheesh A, Muthukumar P, Dewan A. Computational study of metal hydride cooling system. Int J Hydrogen Energy 2009;34:3164–72. http://dx.doi.org/10.1016/j.ijhydene.2009.01.083.
[25] Linder M, Kulenovic R. An energy-efficient air-conditioning system for hydrogen driven cars. Int J Hydrogen Energy

Please cite this article in press as: Talagañis BA, et al., Modeling and optimal design of cyclic processes for hydrogen purification using hydride-forming metals, International Journal of Hydrogen Energy (2014), http://dx.doi.org/10.1016/j.ijhydene.2014.09.045

2011;36:3215–21. http://dx.doi.org/10.1016/j.ijhydene.2010.11.101.
[26] Lototsky MV, Williams M, Yartys VA, Klochko YV, Linkov VM. Surface-modified advanced hydrogen storage alloys for hydrogen separation and purification. J Alloys Compd 2011;509(Suppl. 2):S555–61. http://dx.doi.org/10.1016/j.jallcom.2010.09.206.
[27] Miura S, Fujisawa A, Ishida M. A hydrogen purification and storage system using metal hydride. Int J Hydrogen Energy 2012;37:2794–9. http://dx.doi.org/10.1016/j.ijhydene.2011.03.150.
[28] Au M, Chen C, Ye Z, Fang T, Wu J, Wang O. The recovery, purification, storage and transport of hydrogen separated from industrial purge gas by means of mobile hydride containers. Int J Hydrogen Energy 1996;21:33–7. http://dx.doi.org/10.1016/0360-3199(95)00044-E.
[29] Suzuki K, Ishikawa K, Aoki K. Degradation of $LaNi_5$ and $LaNi_{4.7}Al_{0.3}$ hydrogen-absorbing alloys by cycling. Mater Trans JIM 2000;41:581–4. http://dx.doi.org/10.2320/matertrans1989.41.581.
[30] Ahn H-J, Lee J-Y. Intrinsic degradation of $LaNi_5$ by the temperature induced hydrogen absorption–desorption cycling. Int J Hydrogen Energy 1991;16:93–9. http://dx.doi.org/10.1016/0360-3199(91)90035-H.
[31] Chen XY, Wei LX, Deng L, Yang FS, Zhang ZX. A review on the metal hydride based hydrogen purification and separation technology 2014;448–453.
[32] Talagañis BA, Meyer GO, Aguirre PA. Modeling and simulation of absorption–desorption cyclic processes for hydrogen storage-compression using metal hydrides. Int J Hydrogen Energy 2011;36:13621–31. http://dx.doi.org/10.1016/j.ijhydene.2011.07.139.
[33] Brooke A, Kendrick DA, Meeraus A, Rosenthal RE. GAMS: a user's guide. Scientific Press; 1988.
[34] Laurencelle F, Goyette J. Simulation of heat transfer in a metal hydride reactor with aluminium foam. Int J Hydrogen Energy 2007;32:2957–64. http://dx.doi.org/10.1016/j.ijhydene.2006.12.007.
[35] Handbook of chemical hazard analysis procedures. Federal Emergency Management Agency; 1989.

Please cite this article in press as: Talagañis BA, et al., Modeling and optimal design of cyclic processes for hydrogen purification using hydride-forming metals, International Journal of Hydrogen Energy (2014), http://dx.doi.org/10.1016/j.ijhydene.2014.09.045